JOURNAL OF PROPULSION AND POWER
Vol. 30, No. 2, March–April 2014

Ignition Transients in a Scramjet Engine with Air Throttling Part 1: Nonreacting Flow

Jian Li,* Liwei Zhang,† Jeong Yeol Choi,‡ and Vigor Yang§
Georgia Institute of Technology, Atlanta, Georgia 30332
and
Kuo-Cheng Lin¶
Taitech, Inc., Beavercreek, Ohio 45430

DOI: 10.2514/1.B34763

Achieving efficient ignition and stable combustion in a high-speed environment has long been a serious concern in the development of scramjet engines. In the engine startup stage, the low chamber pressure and unsettled fuel–air mixing tend to blow off the flame, even if a flameholding device such as a cavity is employed. The problem may be circumvented by modulating the flow structures in the isolator and combustor through air throttling downstream of the flameholder. In experiments, compressed air is introduced in a controlled manner into the combustor to generate a precombustion shock train in the isolator. The resultant increases in the temperature and pressure of the airstream in the combustor, along with the decrease in the flow velocity, lead to smooth and reliable ignition. The incidentally formed separated flows adjacent to the combustor sidewall improve fuel–air mixing as a result of enhanced flow distortion and increased residence time. Because insufficient reaction heat release often leads to an unstable shock train, and exceedingly large heat release may cause severe flow spillage or even inlet unstart, dynamic optimization of the throttling operation is needed to ensure the creation of flow conditions conducive to efficient ignition. The present work establishes an integrated theoretical/numerical framework, within which the influences of all known effects on the engine ignition transient and flame development are studied systematically. Part 1 of the study focuses on nonreacting flow development and fuel–air mixing under the influence of air throttling.

Nomenclature

A	=	duct cross-sectional area
H	=	duct height
k	=	turbulent kinetic energy
M	=	Mach number
$\dot{m}$	=	mass flow rate
p	=	pressure
S	=	source terms for k and ω equations
T	=	temperature
u, v, w	=	velocity components
W	=	duct width
x, y, z	=	spatial coordinates
Y	=	mass fraction
η_m	=	fuel–air mixing efficiency
μ	=	viscosity
ρ	=	density
τ	=	viscous stress
Ω	=	vorticity magnitude
ω	=	specific turbulence dissipation rate
$\dot{\omega}$	=	mass production rate due to chemical reactions

Subscripts

A	=	property of air
air	=	property for main air flow
c	=	property of cavity
F	=	property of fuel
i	=	property of species i
k	=	property for k equation
ST	=	stoichiometric proportion of the fuel–air composition
th	=	property for air throttling
w	=	property on solid wall
ω	=	property for ω equation

I. Introduction

IN RECENT years, there has been considerable interest in hydrocarbon-fueled scramjet propulsion [1,2]. Compared with hydrogen, hydrocarbon fuels offer such advantages as high volumetric energy density, low cost, and relative simplicity of operation. The longer residence time required for vaporization, mixing, and completion of chemical reactions in hydrocarbon fuels, however, poses challenges in engine development. The situation is further complicated by issues associated with the active cooling of various parts of the engine; the available cooling technologies typically limit flight Mach number to the range of 4–8 [1,2].

Rapid fuel–air mixing and effective ignition are two prerequisites to achieving efficient combustion in a practical engine flowpath. Transverse fuel injection provides reasonable penetration and mixing, but at the expense of shock losses [2–5]. Many fuel injection schemes, notably, parallel and angled injection from a wall ramp or a strut [6,7], have been proposed and implemented to offer an optimum tradeoff between flow losses and mixing improvement. Techniques such as fuel preheating and the use of hydrogen or silane pilot flames have also been considered, in efforts to enhance the ignition characteristics and flame anchoring capability. The currently available methods are, however, of limited adaptability and do not always give satisfactory results.

During the engine startup stage, the low chamber pressure and unsettled fuel–air mixing tend to blow out the flame, even when a

Received 16 August 2012; revision received 19 August 2013; accepted for publication 20 August 2013; published online 20 February 2014.

*Graduate Research Assistant, formerly at Department of Mechanical Engineering, Pennsylvania State University.
†Postdoctoral Fellow, School of Aerospace Engineering. Member AIAA.
‡Visiting Professor. Member AIAA.
§William R. T. Oakes Professor and Chair, School of Aerospace Engineering; vigor.yang@aerospace.gatech.edu. Fellow AIAA (Corresponding Author).
¶Senior Research Scientist, 1430 Oak Court, Suite 301. Associate Fellow AIAA.

flameholding device such as a cavity [8,9], or an ignition-enhancement device such as a plasma torch [10], is employed. To circumvent this difficulty, much effort has been devoted to modulating the flowfield in the isolator and combustor by imposing a flow blockage downstream of the flameholder, to slow the flow and establish a proper precombustion shock train in the isolator. The blockage mechanism may be mechanical (e.g., insert or butterfly valve) [11], aerodynamic (e.g., air throttle) [12], or thermal (e.g., pyrophoric material such as silane). The resultant increases in the temperature and pressure of the airstream in the combustor, along with the decrease in the flow velocity, lead to smooth and reliable ignition. Furthermore, the incidental flow separation near the wall and in the corner region promotes fuel–air mixing due to enhanced flow distortion and residence time.

Several experimental and numerical studies have been conducted to help understand the isolator aerodynamics in the presence of flow throttling in the downstream region. Waltrup and Billig [13,14] explored the shock structures and developed a correlation for the length of the shock train in a cylindrical duct. Similar problems were examined by Om and Childs [15] and Carroll and Dutton [16] for circular and rectangular ducts, respectively. Emphasis was placed on the details of the flow characteristics of multiple shock wave/turbulent boundary-layer interactions. The flow Mach numbers of concern were in the transonic regime. Lin et al. [17] investigated shock-train structures in constant-area isolators. A throttle valve was installed downstream of the isolator to vary the shock location. Tan and Sun [18] performed wind-tunnel tests to explain the shock properties in a variable-area diffuser. The shock train in a curved diffuser was found to be considerably longer than its counterpart in a straight diffuser. Tam et al. [19] performed numerical studies on the effects of boundary-layer bleed in a rectangular scramjet isolator. Placing slots to remove low-momentum flows near the corners improved isolator performance and shifted the shock train downstream.

Until now, most of the studies have been concerned with either isolator aerodynamics and fuel–air mixing or flame stability under conditions with or without air throttling. No study has thus far addressed the flow and flame evolution during the ignition transient along the entire engine flowpath. The present work attempts to establish an integrated theoretical/numerical framework within which the influences of all known effects on the scramjet engine ignition transient and flame development can be treated systematically. The results obtained will be applicable to the development of active combustor control techniques [20,21]. The physical model simulates an experimental facility operated at the Air Force Research Laboratory, Wright–Patterson Air Force Base [22]. The study comprises two parts. Part 1 deals with the effect of air throttling on the flow evolution in the isolator and ensuing fuel–air mixing in the combustor. Part 2 considers the ignition transient and flame development under conditions with and without air throttling. The present paper is structured as follows. Section II summarizes the theoretical formulation and numerical method for treating unsteady three-dimensional, chemically reacting flows with finite rate chemistry. Section III describes the system configuration and operation. The computational grid and boundary conditions are introduced in Sec. IV. Section V presents results and offers a discussion of the detailed flow development driven by air throttling. Special attention is given to fuel–air mixing and subsequent distribution in the combustor. Conclusions are drawn in Sec. VI.

II. Theoretical Formulation and Numerical Method

The theoretical formulation is based on the complete conservation equations of mass, momentum, energy, and species transport in three dimensions [23–25]. The analysis accommodates finite rate chemical kinetics and variable thermophysical properties for a multicomponent chemically reacting flow. The two-step global kinetics scheme proposed by Westbrook and Dryer [26] is adopted, in light of its simplicity and reasonably accurate modeling of burnt gas containing incompletely oxidized species of hydrocarbon fuels. The effect of turbulent mixing on combustion is treated using the eddy-dissipation model proposed by Magnussen and Hjertager [27]. Turbulence closure is achieved by means of Menter's shear-stress transport (SST) model [28], calibrated for high-speed compressible flows. The model incorporates the standard k-ε model, which is suitable for shear-layer flows, and the Wilcox k-ω model [29] for wall turbulence effects. To save computational cost and expedite calculations, the wall-function concept proposed by Launder and Spalding [30] is implemented to determine the flow velocity near the wall empirically. The overall approach has proven to be adequate, with sufficient numerical grid resolution [25].

A finite volume method is used for numerical discretization. The convective fluxes are evaluated by means of Roe's flux-difference splitting method derived for multispecies reacting flows [31]. MUSCL is employed for high-order spatial accuracy, along with a minmod slope limiter for the total-variation-diminishing (TVD) properties. This spatial discretization strategy satisfies the TVD conditions and features a high-resolution shock-capturing capability. The discretized equations are temporally integrated using a four-stage Runge–Kutta scheme. Further efficiency is achieved with the implementation of a parallel computing technique based on the message-passing-interface library.

The overall approach was validated against several benchmark problems, for which either analytical solutions or experimental data were available [25]. The ability of the numerical scheme to capture steep gradients and shock discontinuities was verified by computing supersonic flows over wedges of different inclinations. In addition, confidence in the turbulence closure based on the Menter SST model was established by calculating near-wall flow properties for a flat-plate boundary layer. Results showed good agreement with experimental measurements in terms of the skin-friction coefficient.

III. System Configuration and Operating Conditions

The physical model of concern, a direct-connect scramjet combustor test facility operated at the Air Force Research Laboratory, is shown in Fig. 1. It includes a facility (inlet) nozzle, an isolator, a combustor equipped with a recessed-cavity flameholder, and an exhaust nozzle. The entire system measures 1789 mm in length. The isolator has a constant-area cross section with an entrance height of 38.1 mm. The combustor starts with a short constant-area section, followed by a channel with a divergence angle of 2.6 deg. The cavity is located on the divergent top wall and its leading edge is 213.7 mm downstream of the combustor entrance. It is 16.7 mm deep, with a base of 65.2 mm length, and a closeout ramp of 22.5 deg. Gaseous ethylene is injected from inclined circular fuel injectors, flush mounted on the top (I-1 and I-2) and bottom (I-3 and I-4) walls upstream of the cavity, designated as the body and cowl sides, respectively. The injection angle is 15 deg from the wall. Throttling air is discharged from a three-section slit with a width of 3.2 mm and a length of 25.4 mm for each section (76.2 mm for the entire three-section slit). The slit is oriented normal to the main airflow and is located on the body-side (top) surface about 100 mm downstream of the cavity. The test rig is capable of simulating flight conditions in the Mach number range of 3.5–6.0 at a dynamic pressure of 24–96 kPa (500–2000 psf).

Figure 2 shows the facility operation sequence under conditions with and without air throttling. The operation starts with the delivery of airflow through the entire system. Once the flowfield has reached its steady state, the fuel injectors are turned on. Air throttling is then activated after a short period. Compressed air is introduced in a controlled manner through the air throttle to generate a precombustion shock train in the isolator. Ignition follows in the combustor, and air throttling is terminated after the flame has been established. The heat release and associated pressure rise in the combustor maintain a stable shock train, as required for sustaining combustion. Insufficient heat release leads to an unstable shock train, and a premature removal of air throttling often results in flame blowout.

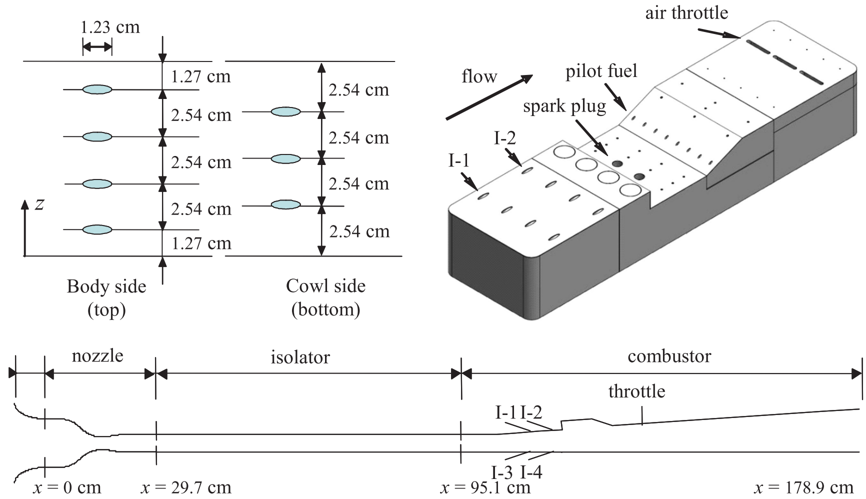

Fig. 1 Scramjet facility flowpath with injection block, cavity flameholder, and air throttle block on the body wall.

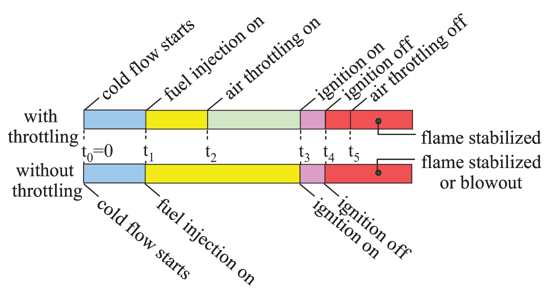

Fig. 2 Facility operation sequence with and without air throttling.

IV. Computational Grid and Boundary Conditions

The computational domain covers the entire facility, from the entrance of the inlet nozzle to the combustor exit. Only one-half of the flowfield in the spanwise direction is considered, to reduce the computational burden. The domain is divided into 164 blocks, to handle the irregular geometry and to facilitate parallel computation. A total of 32.5 million structured grid points are employed, of which 27.2 million ($1654 \times 95 \times 173$) grid points are for the main flowpath and 5.3 million ($361 \times 85 \times 173$) are in the cavity. The numerical grids are clustered toward the walls, with $y^+ \approx 2$ for the first point to resolve the steep flow gradients in the boundary layers.

At the inlet of the facility nozzle, stagnation pressure and temperature are set to the experimentally determined values. A one-dimensional approximation to the axial momentum equation is used to determine the pressure, along with the assumption of zero velocities in the vertical and spanwise directions. At the outlet, where the flow is predominantly supersonic, the flow properties are extrapolated from the interior points. All the solid walls are assumed to be adiabatic, and no-slip conditions are enforced. At the fuel injection ports and air throttling slits, the pressure, temperature, and velocity are specified in accordance with the injector geometry and local flow conditions.

V. Results and Discussion

A. Baseline Flowfield

Simulations were first carried out for a case without fuel injection or air throttling. The total temperature and total pressure at the entrance of the facility nozzle were set to 1106.7 K (1992°R) and 3.51 atm (51.6 psi), respectively, simulating a flight Mach number of 5 and a dynamic pressure of 24 kPa (500 psf) [22]. The air mass flow rate was 0.757 kg/s. The airflow at the entrance of the isolator had a static temperature of 560 K, a static pressure of 0.328 atm, and an axial velocity of 1045 m/s. The corresponding Mach number was 2.2.

Figure 3 shows the distributions of static pressure p_w on the sidewall and Mach number along the centerline under steady conditions. The corresponding facility flowpath is shown at the top of the figure. Supersonic air enters the constant-area duct of the isolator and slows down due to the viscous boundary layers on the walls. It then accelerates at $x = 1.03$ m from a Mach number of 1.8 at the entrance of the divergent duct to a Mach number of 2.1 at the combustor exit. Owing to the flow expansion near the cavity front

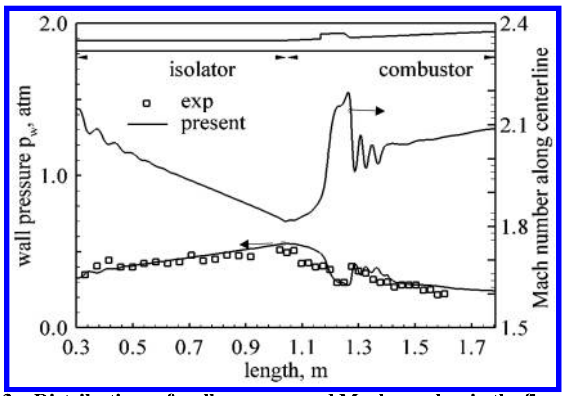

Fig. 3 Distributions of wall pressure and Mach number in the flowpath under steady-state conditions without air throttling.

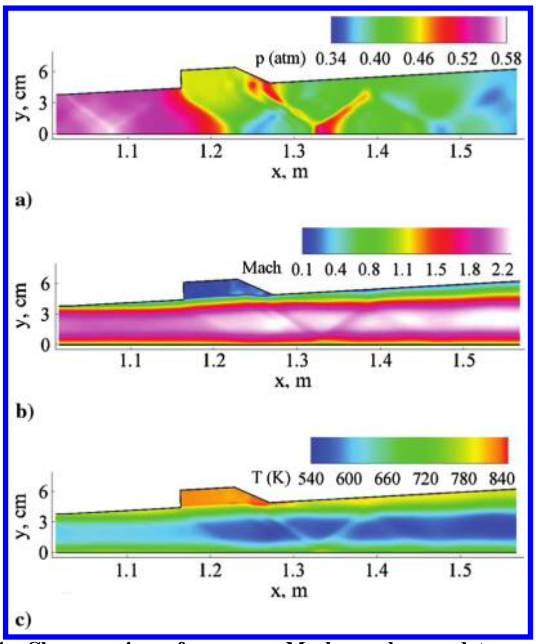

Fig. 4 Close-up view of pressure, Mach number, and temperature contours on x-y plane ($z/W = 1/2$) in combustor section under steady-state conditions without air throttling.

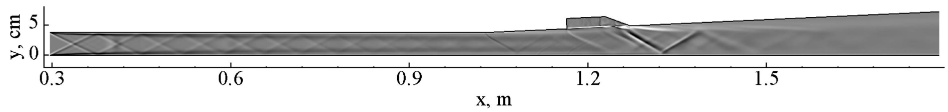

Fig. 5 Shadowgraph of flowfield along entire channel on x-y plane ($z/W = 1/2$) under steady-state conditions without air throttling.

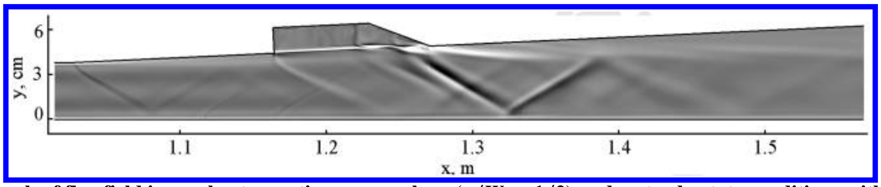

Fig. 6 Shadowgraph of flowfield in combustor section on x-y plane ($z/W = 1/2$) under steady-state conditions without air throttling.

edge, a local peak Mach number of 2.2 is achieved where the static wall pressure drops. The pressure decreases along the cavity bottom wall to a local minimum value at the rear ramp wall, where the shear layer experiences recompression, which produces higher pressure at the trailing edge. Good agreement with the measured wall pressure is obtained. More information about the experiment is available in [22].

Figure 4a shows the static pressure distribution in the combustor on the x-y plane at the midchamber location ($z/W = 1/2$). The rear-facing step of the cavity produces an expansion wave at the leading edge that reduces the local pressure in the high-speed flow stream. The free shear layer then deflects further into the cavity and is finally recompressed on the inclined rear ramp of the cavity. The shear layer impingement on the inclined rear ramp facilitates air entrainment into the cavity, but the consequent pressure drop over the cavity increases the viscous drag in the combustor section. Figure 4b shows the Mach number distribution. The flow is predominantly supersonic and continues to accelerate in the divergent channel. A free shear layer divides the high-momentum airstream from the low-momentum recirculating flow in the cavity. Figure 4c shows the temperature distribution. It has a value of 640 K at the entrance of the combustor

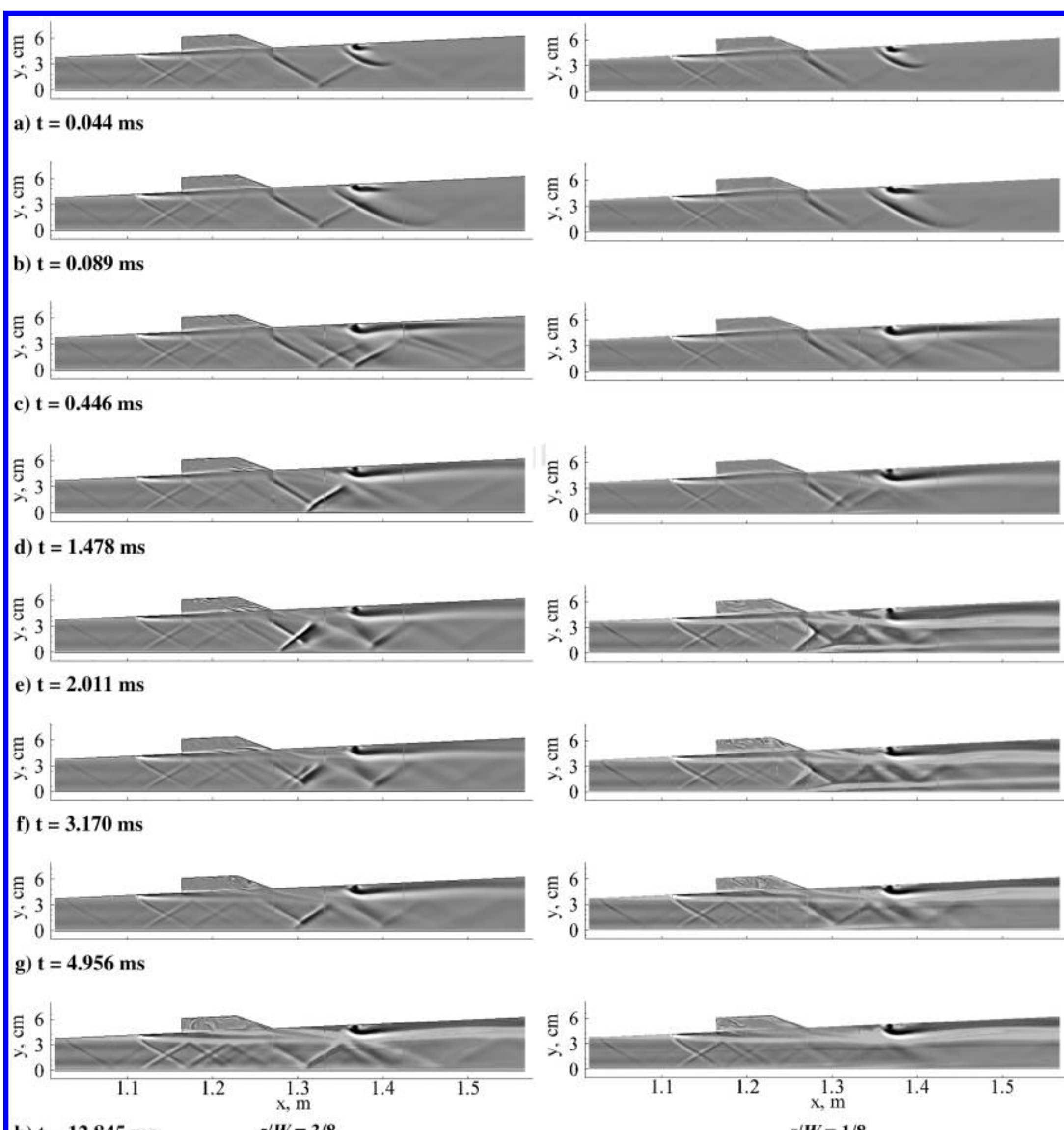

Fig. 7 Shadowgraph of flow evolution on x-y planes at two different spanwise locations ($z/W = 3/8$ and $1/8$) in combustor section with air throttling.

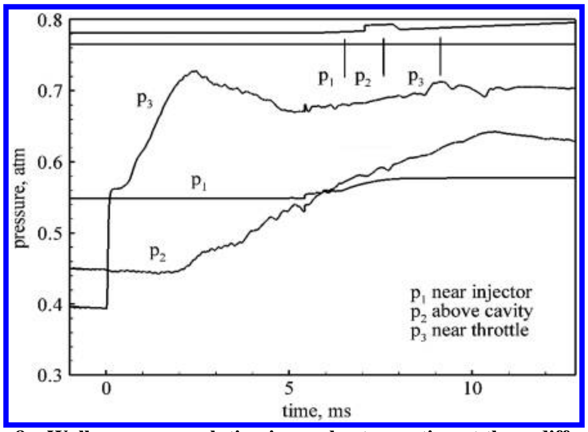

Fig. 8 Wall-pressure evolution in combustor section at three different locations with air throttling.

and then decreases in the divergent section as a consequence of flow expansion. The high temperature (over 800 K) in the cavity is attributed to the local low-momentum flow condition. The presence of the reattached shock wave at the trailing edge of the cavity causes the temperature to reach a local maximum.

Figure 5 shows a shadowgraph of the flowfield along the entire channel on the x-y plane at the midchamber location ($z/W = 1/2$). A close-up view of the combustor region is given in Fig. 6. A free shear layer forms at the leading edge of the cavity, separating the supersonic mainstream from the subsonic flow in the cavity. The flow compression at the end of the cavity results in formation of an oblique shock wave, which then reflects downstream from the cowl-side wall. A series of shock/compression waves are thus produced, reducing in intensity with each reflection. The boundary layer grows rapidly in the divergent section downstream of the cavity, with an accelerating main flow.

Once a steady airflow is established, gaseous ethylene is delivered from the four I-2 and three I-4 injectors into the chamber on both the body and cowl sides, as shown in Fig. 1. In the present study, a fueling split of 60/40 between the I-2 and I-4 injectors is chosen as the baseline case. All the injectors are located at an axial location of $x = 1.11$ m. The total mass flow rates of air in the mainstream and fuel from the injectors are 0.757 and 0.031 kg/s, respectively, corresponding to an overall fuel–air equivalence ratio of 0.6.

B. Effect of Air Throttling

Air throttling is activated after the injected fuel is well mixed with the airstream. The throttling air is choked at the discharge slit. It has a static temperature of 273 K and a static pressure of 1.92 atm. The mass flow rate of 0.151 kg/s amounts to 20% of the mainstream mass flow rate.

Figure 7 shows shadowgraphs of the temporal evolution of the flow structures in the combustor section with air throttling. Throttling air is discharged at $t = 0.0$ ms. A bow shock immediately forms upstream of the slit ($t = 0.044$ ms). As the backpressure rises downstream, the bow shock develops further and expands, reaching the cowl-side wall at $t = 0.089$ ms. Downstream of the bow shock, the boundary layer separates, because of the growing adverse pressure gradient. The bow shock becomes an oblique shock and is pushed upstream as the separation region grows. At $t = 1.478$ ms, the oblique shock merges with the attached shock wave originating from the rear edge of the cavity. The enhanced adverse pressure gradient downstream of the oblique shock then leads to boundary-layer separation on the cowl-side wall. The backpressure-driven oblique shock wave propagates upstream and reaches the trailing edge of the cavity at $t = 2.011$ ms. The lifting of the shear layer over the cavity between $t = 3.17$ and $t = 12.8$ ms is caused by the steepened pressure gradient. After the flowfield has settled down, a series of oblique shocks forms between the boundary layer and the shear layer.

The effects of the sidewall on the flow development can be visualized in the snapshots at the spanwise location of $z/W = 1/8$. The plane cuts through the outermost I-2 injector on the body wall, which is adjacent to the sidewall. The boundary-layer separation on

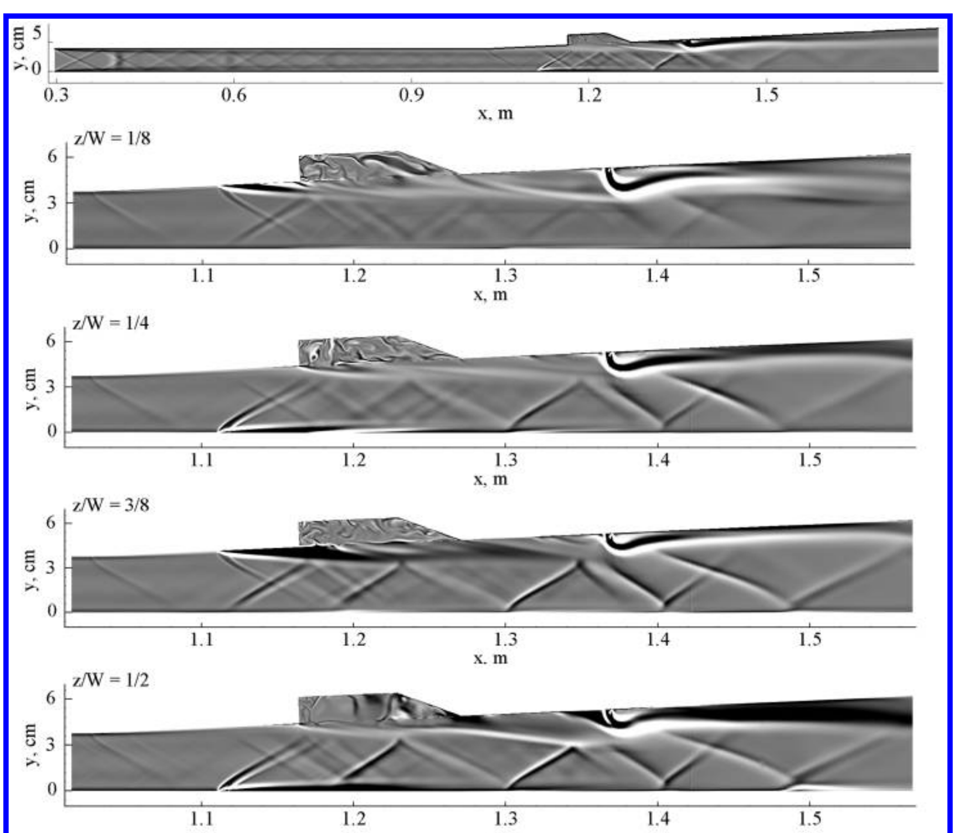

Fig. 9 Shadowgraph of flowfield on x-y planes showing entire channel ($z/W = 1/2$) and combustor section ($z/W = 1/8, 1/4, 3/8$, and $1/2$) under steady-state conditions with air throttling.

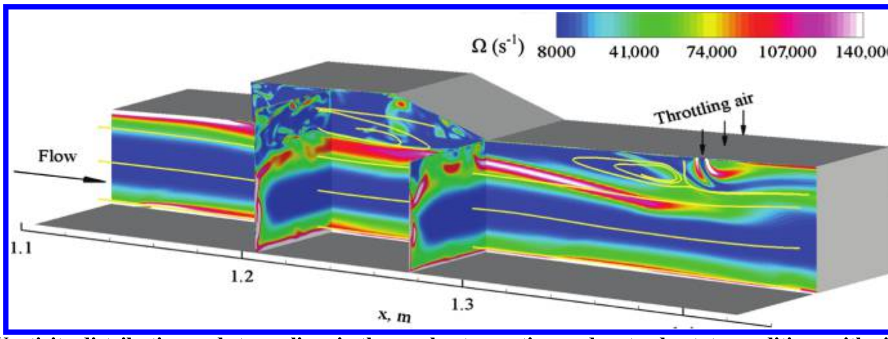

Fig. 10 Vorticity distribution and streamlines in the combustor section under steady-state conditions with air throttling.

both the body and cowl surfaces between the cavity and throttle slit is intensified near the sidewalls.

The static wall pressure was probed at three different axial locations: near the injectors ($x_1 = 1.11$ m), above the cavity ($x_2 = 1.20$ m), and near the throttle slit ($x_3 = 1.36$ m). Figure 8 shows the results. Air throttling drives the wall pressure p_3 to jump from 0.40 to 0.74 atm in a short time period of 2 ms. The resultant increase in the adverse pressure gradient separates the boundary layers from the upstream sidewalls. Shock waves then form and move upstream in response to the rise in backpressure. The wall pressure increase in the vicinity of the cavity and near the injectors upstream of the cavity can be seen in the pressure evolution at p_2 and p_3. Oscillations are observed, due to flow instabilities arising from shock/shear-layer interactions. As the shock waves intersect the shear layer above the rear ramp of the cavity, acoustic fluctuations take place and propagate into the cavity, accompanied by a mass exchange near the cavity trailing edge.

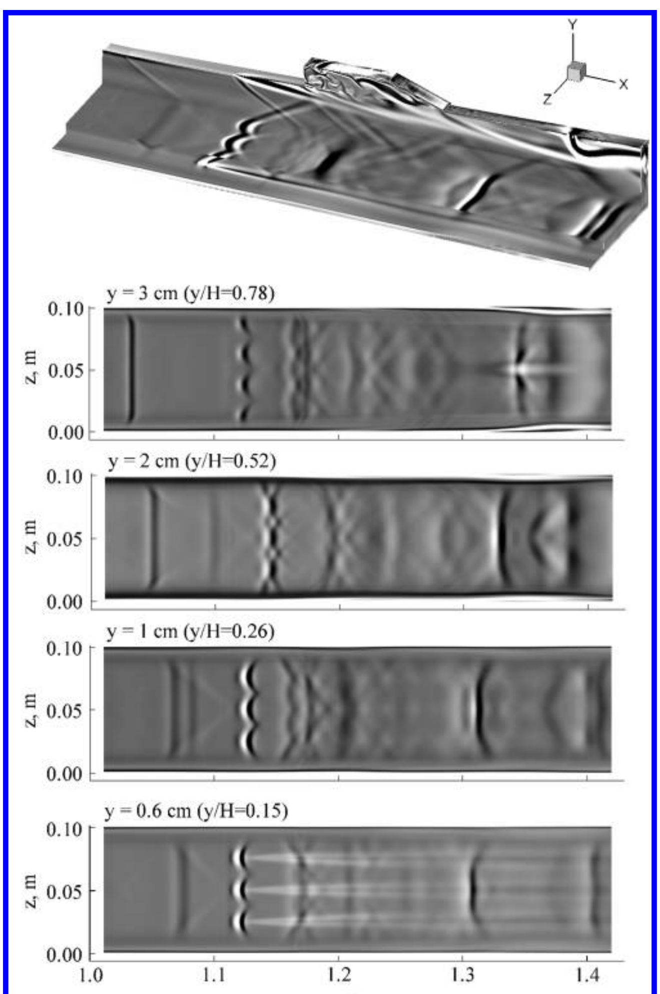

Fig. 11 Shadowgraph perspective view in the combustor section under steady-state conditions with air throttling.

Steady state is achieved after the transient phase, which follows the formation of the shock train in the isolator when the air throttle is switched on. Figure 9 shows shadowgraphs of the flowfield along the entire channel at the midchannel location ($z/W = 1/2$) and in the combustor section at four different spanwise locations ($z/W = 1/8$, $1/4$, $3/8$, and $1/2$) under steady state. Compared with the situation without air throttling shown in Fig. 5, no visible change is observed in the boundary layers and flow structures in the isolator; this suggests that the influence of air throttling on the flowfield is limited to the combustor section. The close-up views of the combustor section indicate the penetration of the throttling air into the supersonic flow. Upstream of the throttle slit, significant boundary-layer separation occurs near the cavity. As a result, the shear layer no longer impinges on the rear edge of the cavity; it is lifted into the downstream separated boundary layer, inducing a series of oblique shocks and compression waves in the mainstream. The interactions between the shock waves and the shear layer produce reattachment-point acoustic oscillations above the rear ramp. This phenomenon is accompanied by enhanced mass exchange and fuel–air mixing at the cavity trailing edge [22,32].

Figure 10 shows the vorticity and streamlines in the combustor section under steady-state conditions with air throttling. Significant recirculation zones are clearly observed. In addition, intense flow separation occurs downstream of the cavity along the body-side wall, due to the local pressure rise from air throttling.

Figure 11 shows a three-dimensional perspective shadowgraph of the steady-state flowfield in the combustor. Four horizontal planes are extracted to reveal detailed flow structures at different vertical locations of $y = 0.6$, 1.0, 2.0, and 3.0 cm, respectively. The inclined fuel injection induces shock waves with bow-shape structures that circle the orifices and cross with the neighboring shocks in the circumferential direction. The bow shock waves from both the body and cowl walls penetrate into the main flow stream, and intersect each other at the height $y = 2$ cm. At a short distance downstream of the orifices, the oblique shock waves reach the wall boundary layers. Further complications in the flowfield arise due to the reflection of these oblique shocks from the combustor walls.

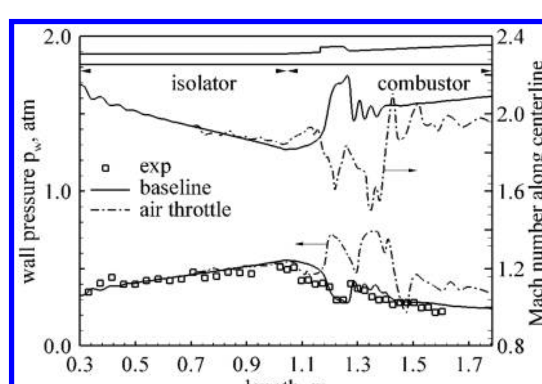

Fig. 12 Distributions of wall pressure and Mach number along the centerline under steady-state conditions with and without air throttling.

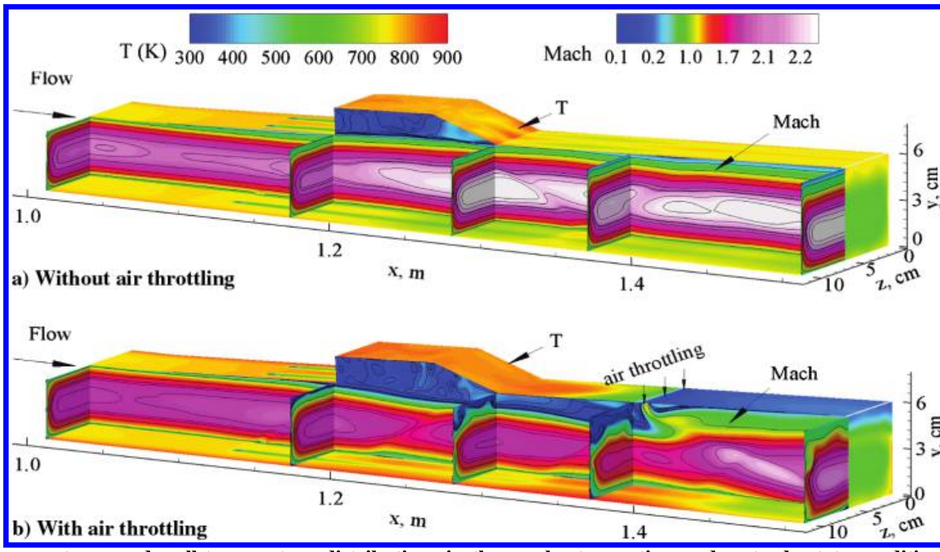

Fig. 13 Mach number contours and wall-temperature distributions in the combustor section under steady-state conditions with and without air throttling.

Figure 12 compares the calculated wall-pressure and Mach number distributions along the flowpath under conditions with and without air throttling. The discharge of throttling air downstream of the combustor provides an aerodynamic blockage mechanism and causes intense flow recompression and boundary-layer separation on the body surface. The backpressure rises significantly to about 0.7 atm. The shear layer is lifted from the cavity, which results in the formation of compression waves, a pressure rise over the cavity, and a decrease in the flow Mach number.

More detailed information about the flow development can be obtained from the Mach number and wall-temperature distributions in Fig. 13. The low-speed flow in the separation zone results in a longer residence time and improved mixing. The boundary-layer separation expands to the corners along the vertical sidewalls and further enhances the mixing of the fuel and airstreams.

The influences of air throttling on the flow evolution and fuel–air mixing in the cavity were studied. As an example, the distribution on a horizontal plane ($\Delta y/H_c = 1/3$), as illustrated schematically in Fig. 14, was considered. Figure 15 shows an almost uniform distribution of the pressure field at about 46 kPa in the absence of air throttling. The situation changes considerably, however, with air throttling. A nonuniform distribution takes place in the range of 61–66 kPa as a consequence of the shock/shear-layer interactions above the cavity. Large pressure variations are also found in the region downstream of the cavity (not shown here), as indicated by the wall-pressure profile in Fig. 12. Figure 16 shows the vorticity-magnitude contours. Air throttling strengthens the vorticity in the bulk of the cavity. The impingement of the shear layer on the rear ramp of the cavity induces flow distortions and hence vorticity generation.

C. Fuel/Air Mixing

The enhancement of the fuel–air mixing in the chamber as a result of air throttling was examined. Figure 17 shows the distributions of the fuel concentration in the flowfield. Semitransparent isosurfaces of ethylene mass fraction are colored at the corresponding concentration scales, so that the images are biased to regions with locally significant fuel distributions. The fuel entrainment into the cavity is significantly different in the cases with and without air throttling, as indicated by the concentration contours. The flowfield without air throttling has a

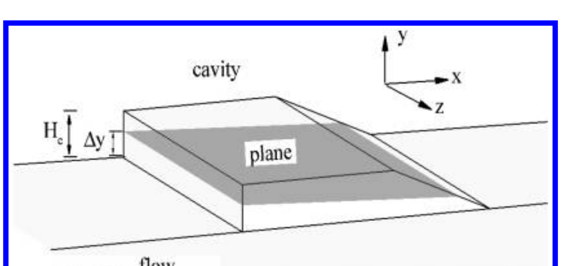

Fig. 14 Schematic of horizontal plane ($\Delta y/H_c = 1/3$) in the cavity.

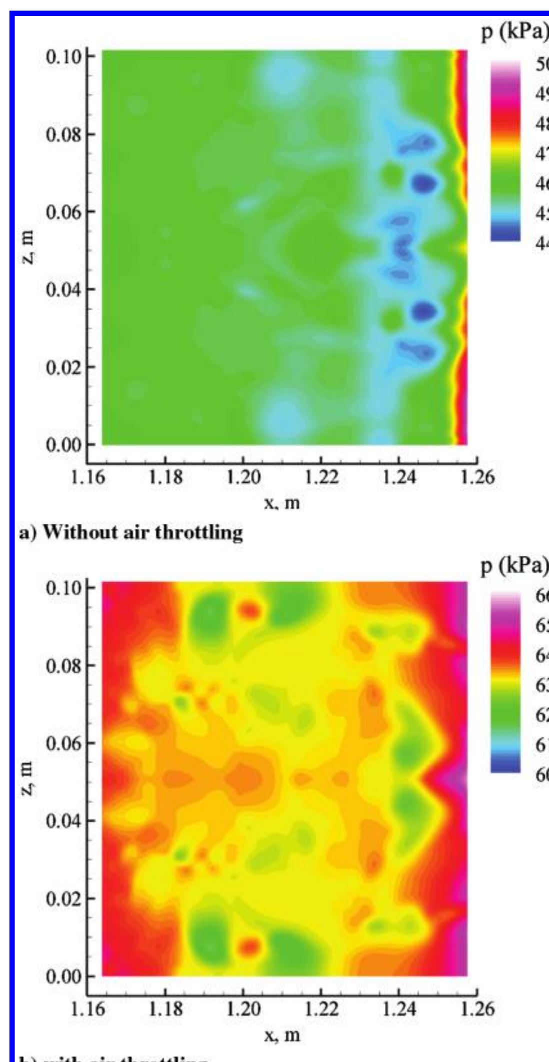

Fig. 15 Pressure contours in the cavity ($\Delta y/H_c = 1/3$) under steady-state conditions with and without air throttling.

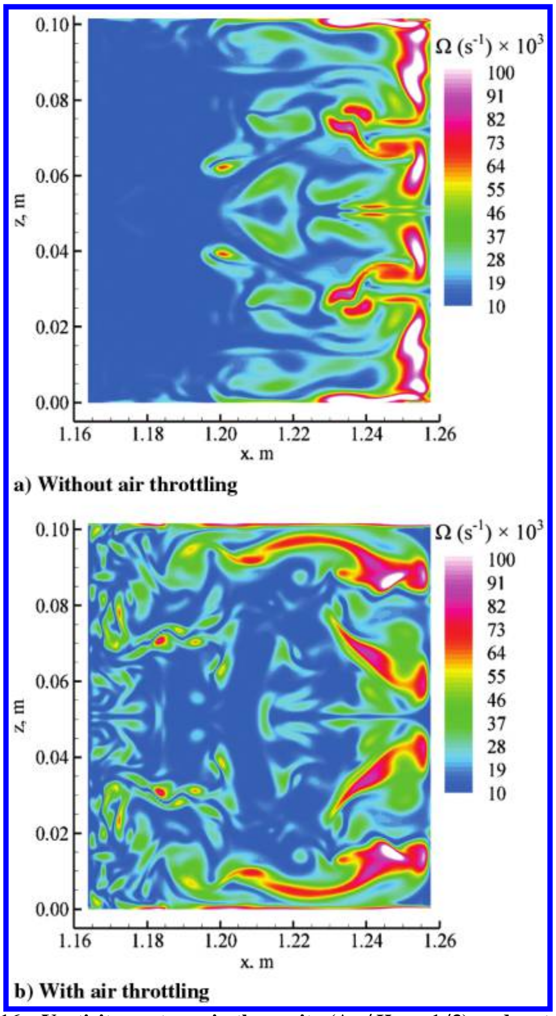

Fig. 16 Vorticity contours in the cavity ($\Delta y/H_c = 1/3$) under steady-state conditions with and without air throttling.

typical ethylene mass fraction of about 2.0–2.5% in the cavity, whereas it reaches over 5.0% in the presence of air throttling.

Figure 18 shows the ethylene distributions on transverse planes at different axial locations. The circular injectors are also shown on both the body- and cowl-side walls. In the baseline case without air throttling, each individual fuel plume remains largely intact, and expands, laterally due to turbulent diffusion and vortex motion downstream. Extensive expansion of the fuel plumes, however, occurs downstream under the influence of air throttling, even leading to interplume mixing in the cavity. The shock-induced boundary-layer separation on the walls distorts the flow and facilitates the fuel spreading in both the vertical and spanwise directions. As a result, the fuel plumes occupy about one-third of the downstream cross-sectional area before they reach the air throttling section ($x/H = 35.5$).

The throttling-induced boundary-layer separation and flow distortions substantially improve the fuel–air entrainment and mixing inside the cavity, as demonstrated by the ethylene distributions in Fig. 19. Without air throttling, only a small fraction of ethylene fuel is entrained into the cavity ($x/H = 30.5 \sim 33.3$). The majority of fuel flows over the cavity and the structure of the individual plumes is maintained downstream. In contrast, the air throttling makes distinct changes in the fuel penetration and diffusion in the combustor section. At the entrance of the cavity, the ethylene fuel starts to expand laterally into the cavity with strong flow convection. The flow separation from the walls lifts the shear layer from the cavity, which then interacts with the shock waves to induce large-scale vorticity and flow distortion in the cavity. As a result, more efficient fuel–air mixing is obtained. The fuel plumes penetrate deeper into the main flow under the influence of shock-induced flow separation, with a significant amount of fuel spreading onto the cowl-side wall.

Figure 20 shows the axial distribution of the mass-weighted streamwise vorticity under conditions with and without air throttling. The quantity is spatially averaged across each transverse plane in the spanwise direction. The vorticity in the cavity is enhanced by the air throttling, as also shown in Fig. 16. The strong oblique shock waves interact with the shear layer over the cavity, further generating vorticity in the wall shear flow. Downstream of the cavity, the flow separation caused by air throttling induces higher vorticity levels, as compared with the baseline flow without throttling. A vorticity spike is clearly observed at $x = 1.36$ m, caused by the throttling air discharge and compression of the main flow near the throttle slit. The maximum at the trailing edge of the cavity in the baseline case is attributed to the interaction between the impinging shear layer and the reattached shock wave.

The fuel–air mixing process can be evaluated quantitatively by the mixing efficiency η_m, defined as the ratio of the fuel that would react (if the mixture temperature passed the ignition point) to the mass flux of the fuel entering the engine [33]. It is expressed as

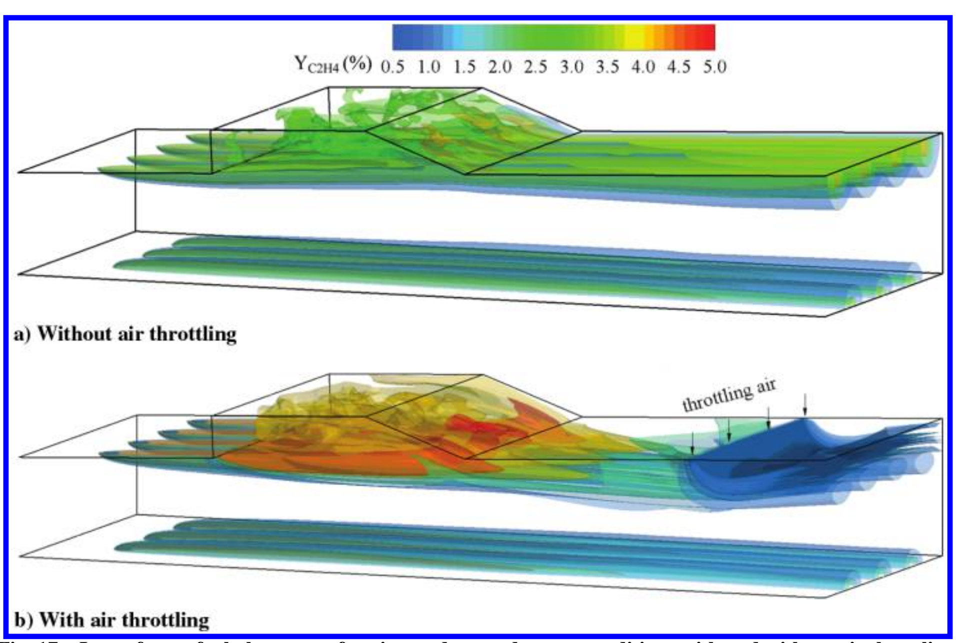

Fig. 17 Isosurfaces of ethylene mass fraction under steady-state conditions with and without air throttling.

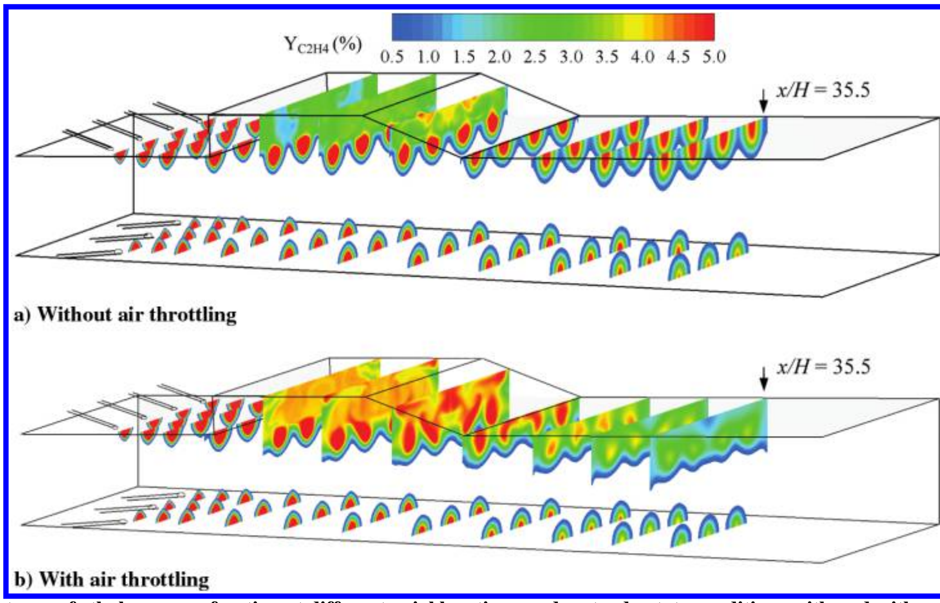

Fig. 18 Contours of ethylene mass fraction at different axial locations under steady-state conditions with and without air throttling.

$$\eta_m = \frac{\dot{m}_{F,\text{mix}}}{\dot{m}_F} = \frac{\int \rho Y_M(\vec{v} \cdot \vec{n})\, dA}{\int \rho Y_F(\vec{v} \cdot \vec{n}))\, dA} \tag{1}$$

where

$$Y_M = \begin{cases} Y_F, & \text{if } Y_F \le Y_T \\ Y_T, & \text{if } Y_F > Y_T \end{cases} \tag{2}$$

and

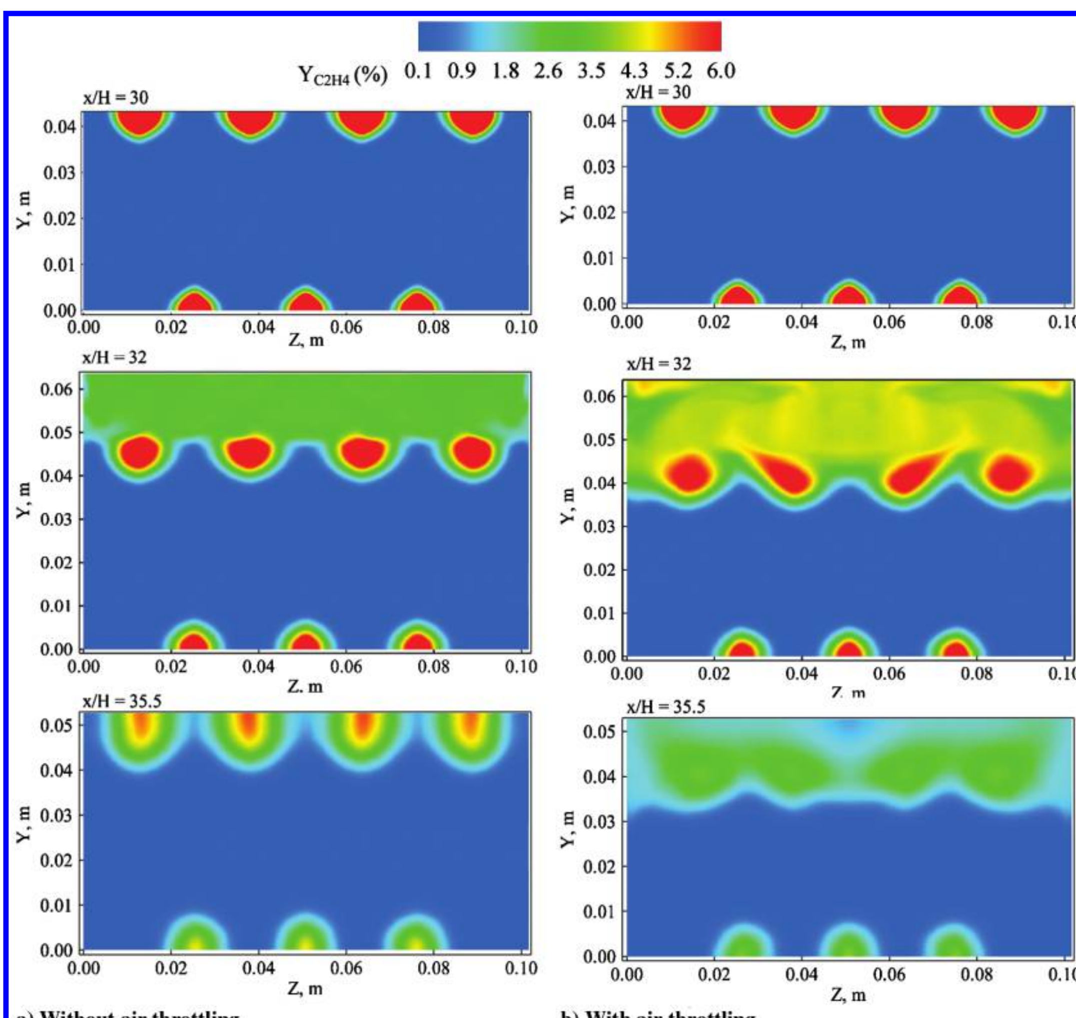

Fig. 19 Distributions of ethylene mass fraction at various axial locations under steady-state conditions with and without air throttling.

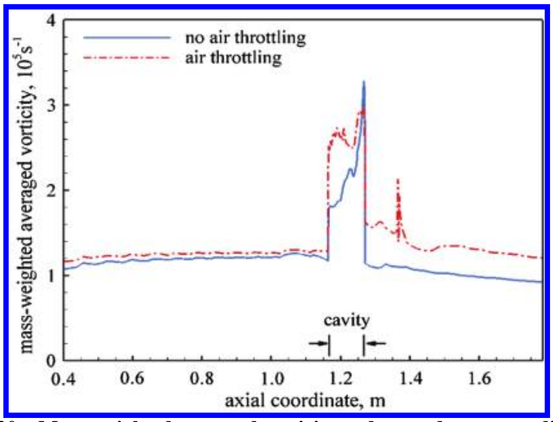

Fig. 20 Mass-weighted averaged vorticity under steady-state conditions with and without air throttling.

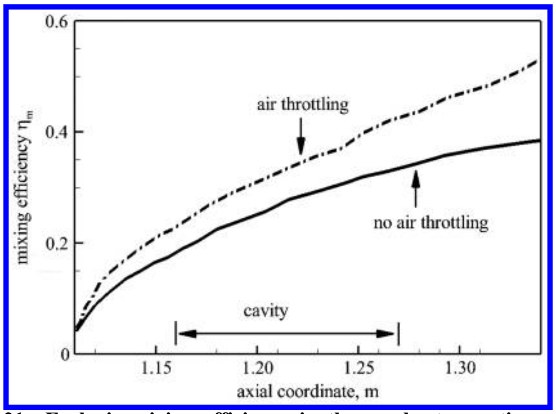

Fig. 21 Fuel–air mixing efficiency in the combustor section under steady-state conditions with and without air throttling.

$$Y_T = Y_A(Y_F/Y_A)_{\mathrm{ST}} \tag{3}$$

where the subscript ST stands for the stoichiometric proportion of the fuel–air composition. In the preceding equations, ρ, A, Y_F, and Y_A represent the density, cross-sectional area, and mass fractions of ethylene fuel and air, respectively.

Figure 21 shows the axial distributions of the mixing efficiency under conditions with and without air throttling. Compared with the baseline flow, a substantial increase in the fuel–air mixing efficiency occurs downstream of the injectors in the presence of air throttling. The mixing, however, is only slightly improved through the separated boundary layer upstream of the cavity (not shown). Air throttling strengthens the low-momentum flow inside the cavity, and more ethylene fuel is entrained into the cavity. Downstream of the cavity, mixing enhancement is primarily caused by the stronger flow distortion and increased residence time along the boundary layers on the walls.

VI. Conclusions

A comprehensive theoretical and numerical framework has been developed to study the flow development and fuel–air mixing in a scramjet engine test facility. The system is equipped with inclined circular fuel injectors, a cavity flameholder, and a three-section air throttle slit. Conditions with and without air throttling have been investigated systematically.

The analysis is based on the complete conservation equations in three dimensions and accommodates finite rate chemical kinetics and variable thermophysical properties for a multicomponent chemically reactive system. Turbulence closure is achieved by means of Menter's shear-stress transport model calibrated for high-speed compressible flows. The overall approach has been benchmarked against several well-defined problems and measured wall-pressure distributions. For the baseline case without air throttling, fuel–air entrainment and mixing inside the cavity is fairly effective. The situation is, however, considerably improved in the presence of air throttling. A series of oblique shock waves is generated in the combustor section due to the increased backpressure caused by the throttling air. The shock waves separate the wall boundary layers and enhance the fuel spreading in both the vertical and spanwise directions, thereby facilitating the mass transport to the cavity and, subsequently, the fuel–air mixing. Detailed flow evolution and fuel spreading and mixing behaviors are explored systematically. The influence of air throttling on the ignition transient and flame development will be addressed in part 2 of the study.

Acknowledgments

This work was sponsored by the U.S. Air Force Research Laboratory, by the John L. and Genevieve H. McCain Endowment at Pennsylvania State University, and by the William R. T. Oakes Endowment at the Georgia Institute of Technology.

References

[1] Curran, E. T., "Scramjet Engines: The First Forty Years," *Journal of Propulsion and Power*, Vol. 17, No. 6, 2001, pp. 1138–1148. doi:10.2514/2.5875

[2] Segal, C., *Scramjet Engine: Processes and Characteristics*, Cambridge Univ. Press, New York, 2009.

[3] Bushnell, D. M., "Hypervelocity Scramjet Mixing Enhancement," *Journal of Propulsion and Power*, Vol. 11, No. 5, 1995, pp. 1088–1090. doi:10.2514/3.51445

[4] Lavante, V. E., Zeitz, D., and Kallenberg, M., "Numerical Simulation of Supersonic Airflow with Transverse Hydrogen Injection," *Journal of Propulsion and Power*, Vol. 17, No. 6, 2001, pp. 1319–1326. doi:10.2514/2.5881

[5] Bowersox, R. D. W., Fan, H., and Lee, D., "Sonic Injection into a Mach 5.0 Freestream Through Diamond Orifices," *Journal of Propulsion and Power*, Vol. 20, No. 2, 2004, pp. 280–287. doi:10.2514/1.9254

[6] Jacobsen, L. S., Gallimore, S. D., Schetz, J. A., O'Brien, W. F., and Goss, L. P., "Improved Aerodynamic-Ramp Ramp Injector: Injector in Supersonic Flow," *Journal of Propulsion and Power*, Vol. 19, No. 4, 2003, pp. 663–673. doi:10.2514/2.6155

[7] Hsu, K.-Y., Carter, C. D., Gruber, M. R., Barhorst, T., and Smith, S., "Experimental Study of Cavity-Strut Combustion in Supersonic Flow," *Journal of Propulsion and Power*, Vol. 26, No. 6, 2010, pp. 1237–1246. doi:10.2514/1.45767

[8] Ben-Yakar, A., and Hanson, R. K., "Cavity Flameholders for Ignition and Flame Stabilization in Scramjets: An Overview," *Journal of Propulsion and Power*, Vol. 17, No. 4, 2001, pp. 869–877. doi:10.2514/2.5818

[9] Mathur, T., Gruber, M. R., Jackson, K., Donbar, J., Donaldson, W., Jackson, T., and Billig, F., "Supersonic Combustion Experiments with a Cavity-Based Fuel Injector," *Journal of Propulsion and Power*, Vol. 17, No. 6, 2001, pp. 1305–1312. doi:10.2514/2.5879

[10] Kitagawa, T., Moriwaki, A., Murakami, K., Takita, K., and Masuya, G., "Ignition Characteristics of Methane and Hydrogen Using a Plasma Torch in Supersonic Flow," *Journal of Propulsion and Power*, Vol. 19, No. 5, 2003, pp. 853–858. doi:10.2514/2.6175

[11] Gruenig, C., Avrashkov, V., and Mayinger, F., "Self-Ignition and Supersonic Reaction of Pylon-Injected Hydrogen Fuel," *Journal of Propulsion and Power*, Vol. 16, No. 1, 2000, pp. 35–40.

[12] Gruber, M. R., Donbar, J., Jackson, K., Mathur, T., Baurle, R., Eklund, D., and Smith, C., "Newly Developed Direct-Connect High-Enthalpy Supersonic Combustion Research Facility," *Journal of Propulsion and Power*, Vol. 17, No. 6, 2001, pp. 1296–1304. doi:10.2514/2.5878

[13] Waltrup, P. J., and Billig, F. S., "Structure of Shock Waves in Cylindrical Ducts," *AIAA Journal*, Vol. 11, No. 10, 1973, pp. 1404–1408. doi:10.2514/3.50600

[14] Waltrup, P. J., and Billig, F. S., "Prediction of Precombustion Wall Pressure Distributions in Scramjet Engines," *Journal of Spacecraft and Rockets*, Vol. 10, No. 9, 1973, pp. 620–622. doi:10.2514/3.27782

[15] Om, D., and Childs, M. E. "Multiple Transonic Shock-Wave/Turbulent Boundary-Layer Interaction in a Circular Duct," *AIAA Journal*, Vol. 23, No. 10, 1985, pp. 1506–1511.
doi:10.2514/3.9117

[16] Carroll, B. F., and Dutton, J. C., "Characteristics of Multiple Shock Wave/Turbulent Boundary-Layer Interactions in Rectangular Ducts," *Journal of Propulsion and Power*, Vol. 6, No. 2, 1990, pp. 186–193.
doi:10.2514/3.23243

[17] Lin, K. C., Tam, C. J., Jackson, K. R., Eklund, D. R., and Jackson, T. A., "Characterization of Shock Train Structures Inside Constant-Area Isolators of Model Scramjet Combustors," AIAA Paper 2006-816, 2006.

[18] Tan, H., and Sun, S., "Preliminary Study of Shock Train in a Curved Variable-Section Diffuser," *Journal of Propulsion and Power*, Vol. 24, No. 2, 2008, pp. 245–252.
doi:10.2514/1.31981

[19] Tam, C. J., Eklund, D., Behdadnia, R., and Jackson, T., "Investigation of Boundary Layer Bleed for Improving Scramjet Isolator Performance," AIAA Paper 2005-3286, 2005.

[20] Fung, Y. T., Yang, V., and Sinha, A., "Active Control of Combustion Instabilities with Distributed Actuators," *Combustion Science and Technology*, Vol. 78, Nos. 4–6, 1991, pp. 217–245.
doi:10.1080/00102209108951750

[21] Fung, Y. T., and Yang, V., "Active Control of Nonlinear Pressure Oscillations in Combustion Chambers," *Journal of Propulsion and Power*, Vol. 8, No. 6, 1992, pp. 1282–1289.
doi:10.2514/3.11474

[22] Lin, K. C., Jackson, K., Behdadnia, R., Jackson, T. A., Ma, F. H., and Yang, V., "Acoustic Characterization of an Ethylene-Fueled Scramjet Combustor with a Cavity Flameholder," *Journal of Propulsion and Power*, Vol. 26, No. 6, 2010, pp. 1161–1169.
doi:10.2514/1.43338

[23] Roh, T. S., Tseng, I. S., and Yang, V., "Effects of Acoustic Oscillations on Flame Dynamics of Homogeneous Propellants in Rocket Motors," *Journal of Propulsion and Power*, Vol. 11, No. 4, 1995, pp. 640–650.
doi:10.2514/3.23889

[24] Hsieh, S. Y., and Yang, V., "Preconditioned Flux-Differencing Scheme for Chemically Reacting Flows at All Mach Numbers," *International Journal of Computational Fluid Dynamics*, Vol. 8, No. 1, 1997, pp. 31–49.
doi:10.1080/10618569708940794

[25] Li, J., "Ignition Transient in an Ethylene Fuelled Scramjet Engine with Air Throttling," Ph.D. Thesis, Pennsylvania State Univ., University Park, PA, 2009.

[26] Westbrook, C. K., and Dryer, F. L., "Simplified Reaction Mechanisms for the Oxidation of Hydrocarbon Fuels in Flames," *Combustion Science and Technology*, Vol. 27, Nos. 1–2, 1981, pp. 31–43.
doi:10.1080/00102208108946970

[27] Magnussen, B. F., and Hjertager, B. H., "On Mathematical Models of Turbulent Combustion with Special Emphasis on Soot Formation and Combustion," *Symposium (International) on Combustion*, Vol. 16, No. 1, 1977, pp. 719–729.
doi:10.1016/S0082-0784(77)80366-4

[28] Menter, F. R., "Two-Equation Eddy-Viscosity Turbulence Models for Engineering Applications," *AIAA Journal*, Vol. 32, No. 8, 1994, pp. 1598–1605.
doi:10.2514/3.12149

[29] Wilcox, D. C., *Turbulence Modeling for CFD*, DCW Industries, La Cañada, CA, 1993.

[30] Launder, B. E., and Spalding, D. B., *Mathematical Models of Turbulence*, Academic Press, New York, 1972.

[31] Zhang, L. W., "Flow Dynamics and Scalar Mixing of Transverse Jets into Crossflows," Ph.D. Thesis, Pennsylvania State Univ., University Park, PA, 2011.

[32] Choi, J. Y., Ma, F. H., and Yang, V., "Combustion Oscillations in a Scramjet Engine Combustor with Transverse Fuel Injection," *Proceedings of the Combustion Institute*, Vol. 30, No. 2, 2005, pp. 2851–2858.

[33] Tam, C. J., Hsu, K. Y., Gruber, M. R., and Raffoul, C. N., "Fuel/Air Mixing Characteristics of Strut Injectors for Scramjet Combustor Applications," AIAA Paper 2008-6925, 2008.

C. Segal
Associate Editor